Nuclear Materials and Energy 34 (2023) 101345

Contents lists available at ScienceDirect

Nuclear Materials and Energy

journal homepage: www.elsevier.com/locate/nme

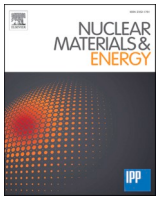

Characterisation of divertor detachment onset in JET-ILW hydrogen, deuterium, tritium and deuterium–tritium low-confinement mode plasmas

M. Groth [a,*], V. Solokha [a], S. Aleiferis [b,c], S. Brezinsek [d], M. Brix [c], I.S. Carvalho [e], P. Carvalho [e,c], G. Corrigan [c], D. Harting [d], N. Horsten [a,f], I. Jepu [g,c], J. Karhunen [c], K. Kirov [c], B. Lomanowski [h], K.D. Lawson [c], C. Lowry [c], A.G. Meigs [c], S. Menmuir [c], E. Pawelec [i], T. Pereira [e], A. Shaw [c], S. Silburn [c], B. Thomas [c], S. Wiesen [d], P. Börner [d], D. Borodin [d], S. Jachmich [j], D. Reiter [k], G. Sergienko [d], Z. Stancar [c], B. Viola [c], P. Beaumont [c], J. Bernardo [c], I. Coffey [c], N.J. Conway [c], E. de la Luna [l], D. Douai [m], C. Giroud [c], J. Hillesheim [c], L. Horvath [c], A. Huber [d], P. Lomas [c], C. F. Maggi [c], M. Maslov [c], C. Perez von Thun [n], S. Scully [c], N. Vianello [o], M. Wischmeier [p], the JET contributors[1]

[a] *Aalto University, Espoo, Finland*
[b] *NCSR Demokritos Institute of Nuclear and Particle Physics, Athens, Greece*
[c] *UKAEA, Culham Science Centre, Abingdon, UK*
[d] *Forschungszentrum Jülich, Institute for Energy and Climate Research Plasma Physics, Jülich, Germany*
[e] *Instituto de Plasmas e Fusão Nuclear, Universidade Tecnica de Lisboa, Lisbon, Portugal*
[f] *KU Leuven, Leuven, Belgium*
[g] *National Institute for Laser Plasma and Radiation Physics, Măgurele, Romania*
[h] *Oak Ridge National Laboratory, Oak Ridge, TN, USA*
[i] *University of Opole, Opole, Poland*
[j] *ITER Organization, St Paul Lez Durance Cedex, France*
[k] *Heinrich-Heine University Düsseldorf, Düsseldorf, Germany*
[l] *Laboratorio Nacional de Fusion, CIEMAT, Madrid, Madrid, Spain*
[m] *CEA, IRFM, F-13108 Saint Paul Lez Durance, France*
[n] *Institute of Plasma Physics and Laser Microfusion (IPPLM), Warsaw, Poland*
[o] *Consorzio RFX, CNR, ENEA, INFN, Università di Padova, Padova, Italy*
[p] *Max Planck Institut für Plasmaphysik, Garching, Germany*

ARTICLE INFO

Keywords:
Detachment
Hydrogen isotopes
JET

ABSTRACT

Measurements of the ion currents to and plasma conditions at the low-field side (LFS) divertor target plate in low-confinement mode plasmas in the JET ITER-like wall materials configuration show that the core plasma density required to detach the LFS divertor plasma is independent of the hydrogenic species protium, deuterium and tritium, and a 40 %/60 % deuterium–tritium mixture. This observation applies to a divertor plasma configuration with the LFS strike line connected to the horizontal part of the LFS divertor chosen because of its superior diagnostic coverage. The finding is independent of the operational status of the JET cryogenic pump. The electron temperature (T_e) at the LFS strike line was markedly reduced from 25 eV to 5 eV over a narrow range of increasing core plasma density, and observed to be between 2 eV and 3 eV at the onset of detachment. The electron density (n_e) peaks across the LFS plasma when T_e at the target plate is 1 eV, and spatially moves to the X-point for higher core densities. The density limit was found approximately 20 % higher in protium than in tritium and deuterium–tritium plasmas.

* Corresponding author at: Aalto University, Otakaari 1, 02150 Espoo, Finland.
E-mail address: mathias.groth@aalto.fi (M. Groth).

[1] See the author list of 'Overview of JET results for optimising ITER operation' by J. Mailloux et al. Nucl. Fusion **62** (2022) 042026.

https://doi.org/10.1016/j.nme.2022.101345
Received 12 June 2022; Received in revised form 25 November 2022; Accepted 19 December 2022
Available online 21 December 2022

1. Introduction

Detachment of the divertor plasma in ITER and in future fusion power plants is a prerequisite for safe operation at high duty cycle ([1,2] and therein). The onset of detachment, i.e., the formation of a cold (electron temperature, $T_e < 3$ eV) and dense (electron density, $n_e > 1x10^{20}$ m^{-3}) plasma region adjacent to the divertor target plates, is characterized by the reduction of the fuel ion fluxes to the divertor target plates compared to the high-recycling, attached regime. In tokamaks, detached regimes are typically achieved when operating at high core plasma density, thus main scrape-off layer (SOL) densities, close to the density limit, often assisted by impurity injection to further cool the divertor plasma. The required degree of detachment in ITER and in future power plants is set by the remaining heat flux to the divertor surface, including plasma surface recombination. E.g., a residual fuel ion flux of $1x10^{24}$ m^{-2} s^{-1} at 2 eV results in 5 MW/m^2, one third of the present upper limit of the heat flux [3], highlighting the need for significant reduction of the fuel ion fluxes beyond what is achieved with radiative cooling only. Understanding and being able to predict the onset and formation of divertor plasma detachment is one of the most critical tasks in magnetic confinement fusion.

Conceptually, the usage of the different hydrogenic isotopes protium (here, H), deuterium (D) and tritium (T), and the homonuclear isotopomer molecules H_2, D_2 and T_2, results in different plasma and neutral conditions in the divertor: for identical plasma conditions, the ionization mean free path, the fuel ion velocity at the target plate and the molecular gas flow through the vacuum system scale with the square root of the isotope mass ratios. E.g., the ionization mean free path of D and T atoms is 0.71 and 0.58 times shorter than that of H atoms, respectively. Furthermore, the sticking probability of hydrogenic molecules on a cryogenic panel is higher for D_2 and T_2 than for H_2 (for the JET divertor cryogenic pump, [4]). In addition, the fuel ion interaction with hydrogenic molecules is anticipated to be isotopomer-dependent as their reaction rates are impacted by the isotopomer mass ([5] and therein). Given these physics models, the plasma-neutral gas is anticipated to rearrange itself for each hydrogen isotope potentially offsetting or amplifying the impact of the isotope species.

Previous experiments in JET with the carbon wall (JET-C) showed for low-confinement mode (L-mode) H, D and T plasmas that the density required for the onset of detachment and the density limit scaled inversely with the fuel ion mass in a vertical divertor plasma configuration (20 % lower for T versus H), while no isotope effect was observed in a horizontal divertor plasma configuration [6]. Measurements in ohmic plasmas the JET ITER-like wall (JET-ILW) indicated a 10 % higher detachment onset density of the low-field side (LFS) divertor plasma for H versus D in a divertor plasma configuration with the high-field side (HFS) strike line on the vertical face of the HFS divertor and the LFS strike line on the horizontal face of the LFS divertor [7]. In contrast, and consistent with the JET-C measurements, a 30 % higher density for the onset of detachment of the LFS divertor plasma for H versus D plasmas was measured in a configuration with the HFS and LFS strike lines on the vertical faces of the HFS and LFS divertor, respectively.

Since JET operation in tritiated plasmas during the 2020–21 tritium and deuterium–tritium experimental campaigns was limited to a daily tritium consumption of 44 bar L of T per run day [8], the T and D-T experiments reported here were carried out with the divertor cryogenic pump panels operated at liquid nitrogen temperature (LN_2, 77 K), at which hydrogenic gases are not pumped. In contrast, in pumped operation the cryogenic pump panels are cooled to super-critical helium temperature (sc-He, 5.2 K, [9]). The cryogenic pump is toroidally symmetric and located in the sub-divertor attached to the radially inner side of divertor coil 4 (see Fig. 1a and Fig. 2 in [9]). The sub-divertor connects to the divertor via toroidally symmetric pump ducts of height 10 cm, including radiation shields (louvres), which determine the vacuum conductance and thus the effective pumping speed of the cryogenic system on the JET vacuum vessel.

2. General plasma description

The fuel ion fluxes to and the plasma conditions at the HFS and LFS target plates, and Lyman and Balmer emission across the LFS divertor volume were measured in H, D, T and D-T L-mode plasmas with the LFS strike line on the horizontal part of the JET divertor at the LFS (Fig. 1). The HFS strike line was placed onto the vertical face of the HFS divertor.

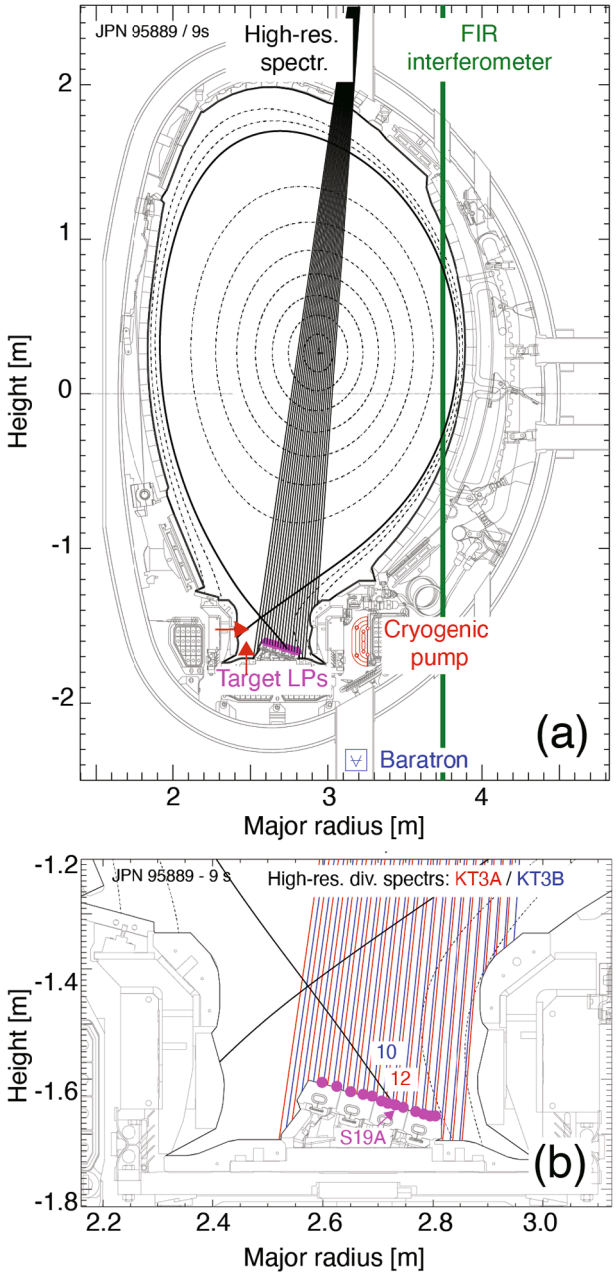

Fig. 1. Full view (a) and divertor view (b) of the JET vessel structures and magnetic equilibrium of JET Pulse Number 95889 at 9 s with the study-relevant components highlighted: locations of the primary gas injection modules (red arrows), cryogenic pump (red), far-infrared interferometer (green), high-resolution divertor spectrometer (black), target Langmuir probes (magenta) and sub-divertor baratron (blue). For the divertor view (b), the divertor spectrometer is further differentiated for system KT3A (red) and KT3B (blue), chords 12 (KT3A) and 10 (KT3B) are highlighted, and Langmuir probe S19A is marked. (For interpretation of the references to colour in this figure legend, the reader is referred to the web version of this article.)

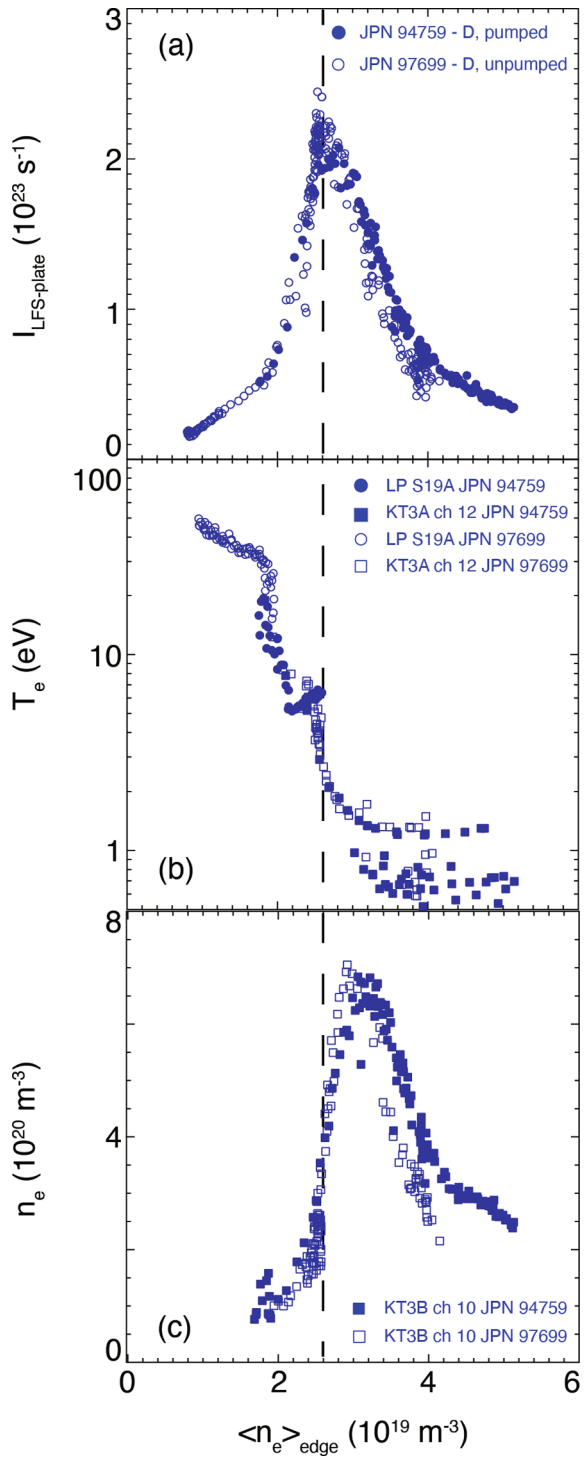

Fig. 2. Total ion current to the LFS target plate (a), electron temperature (b) and electron density (c) as a function of line-averaged density at the outer edge of the core plasma in deuterium plasmas. T_e was measured with Langmuir probes (circles, probe S19A) and inferred spectroscopically (KT3A, squares, channel 12), while n_e was inferred spectroscopically only (KT3B, squares, channel 10). The JET pulse with applied pumping by the cryogenic pump is shown as solid symbol (JPN 94579) and without by the open symbols (JPN 97699). The black dashed vertical line indicates the assumed detachment onset density based on the saturation of $I_{div,LFS-plate}$.

The decision for this divertor plasma configuration was made because of the superior spectroscopic coverage of the horizontal LFS target over the vertical LFS target, despite the indication of a stronger isotope effect in the latter configuration. For all considered plasmas the plasma current (I_P) was 2.5 MA and the toroidal magnetic field (B_T) at the magnetic axis 2.5 T, with the ion **B**x∇B drift pointing into the divertor. Besides ohmic heating (with increasing plasma density 1.6 to 1.9 MW) neutral beam heating of 1.0 to 1.1 MW was applied. Over the course of several campaigns, hydrogen (C37, 2016), deuterium (C28, 2011 and C38, 2019), tritium (C40, 2021) and deuterium–tritium (C41, 2021) plasmas were executed by way of hydrogenic gas only fuelling ramps from low-recycling conditions to the density limit with constant strike line positions. The characterization of the deuterium plasmas was previously reported in [10,11,12]. For the D-T plasmas, a tritium concentration of 55–60 % was inferred spectroscopically across the LFS divertor plasma [13] and in the exhaust gas in the sub-divertor [14]. The absence of significant impurity concentration and radiation, in particular in detached conditions, resulted in plasmas of effective charge state 1.0–1.2 measured in all plasmas, independent of the isotope species. Radiation from beryllium was inferred to be one order of magnitude lower than from the hydrogenic species (dominated by Lyman-α emission) and Bremsstrahlung, and thus negligible [10]. In high-recycling and detached conditions in these plasmas, tungsten sputtering is suppressed [15] and tungsten radiation does not play a role in the power balance of the SOL [10]. Increasing the temperature of the cryogenic pump panels from sc-He to LN_2 for a subset of deuterium plasmas in these studies showed that for the same core plasma density and high-recycling conditions, the D_2 pressure in the sub-divertor increased by a factor of 5 (0.04 Pa to 0.2 Pa). Typically, gas injection rates of 1-2x10^{21} tritons/s – a factor of 100 lower than the recycling ion currents at the target plates – were sufficient in unpumped plasmas to raise the core plasma density from low-recycling conditions to the density limit.

The profiles of ion saturation current densities (j_{sat}) to the LFS plate as measured by Langmuir probes (Fig. 1) are integrated for the total plate-integrated currents (I_{div}); for attached plasma conditions with $T_e \gtrsim$ 5 eV, the Langmuir probes also provided reliable measurements for T_e and n_e. Within the uncertainties of individual Langmuir probes contributing to I_{div}, I_{div} is the least affected target plasma parameter affected by small ($\lesssim$ 5 mm) deviations of the strike line position. Below 5 eV the Langmuir probe measurements for T_e and n_e, thus electron pressure (p_e), at the sheath entrance are found to be unreliable and omitted from the analyses. Spectroscopic measurements of the Balmer series were made with several low and high-resolution instruments [16–18] (Fig. 1), and the line-averaged T_e and n_e across the LFS divertor leg, $<T_e>_{LFS-div}$ and $<n_e>_{LFS-div}$, respectively, were inferred using the fitted continuum emission of the Balmer series and Stark broadening of the Balmer-δ line, respectively [16,17]. These measurements critically extended the T_e and n_e measurements in the divertor to as low as 0.5 eV and 1x10^{21} m^{-3}. The Balmer series emission is spatially resolved by tangentially viewing cameras, which peaked at the LFS strike line region for the high-recycling conditions investigated in these plasmas [11], hence locating the line-averaged T_e and n_e to the vicinity of the LFS strike line region. Note that the Langmuir probe and the spectroscopically inferred electron pressures are complementary, but cannot be assumed the same due to the different plasma regions and plasma conditions for which the methods are valid. Due to the absence of reliable measurements the separatrix location upstream of the divertor X-point, e.g., at the LFS midplane, and thus the plasma conditions at the separatrix, in this publication the line-averaged density in the LFS edge of the main plasma ($<n_e>_{edge}$, see Fig. 1) is used as the primary independent plasma parameter. Previous studies in identical JET-ILW L-mode deuterium plasmas indicated a 2:1 correlation of n_e on the separatrix at the LFS midplane ($n_{e,sep,LFS-mp}$) with $<n_e>_{edge}$, and $T_{e,sep,LFS-mp}$ of approximately 60 eV for all $<n_e>_{edge}$ considered [19]. Given the brevity of report, potential differences in the main SOL profiles due to the isotope mass are deferred to future publications. The suitability of

$<n_e>_{edge}$ as the primary scaling parameter is further justified as, globally, the same radiated power in the core plasma was observed for all isotope species. Hence, for the same ohmic and neutral beam heating power the same power across the separatrix is assumed for all isotope species.

3. Detachment onset of the LFS divertor plasma in deuterium pumped and unpumped conditions

For both states of the cryogenic pump, $<n_e>_{edge}$ at detachment onset was the same density as indicated by the saturation of $I_{div,LFS\text{-}plate}$ and subsequent reduction with $<n_e>_{edge}$ in Fig. 2a. Both T_e measured by a Langmuir probe radially outboard of the LFS strike line, $T_{e,LFS\text{-}plate}$ (Fig. 1), and spectroscopically inferred, $<T_e>_{LFS\text{-}div}$ from a line-of-sight which strikes the target plate at the same probe position (Fig. 1), showed a marked reduction from 25 eV to 5 eV over the range of $<n_e>_{edge}$ from $2.0x10^{19}$ m^{-3} to $2.6x10^{19}$ m^{-3}. Typically, the fitting of the current–voltage characteristics of Langmuir probes for T_e, and thus n_e, becomes unreliable for $T_e < 5$ eV, while the spectroscopic analysis for T_e is challenging for $T_e > 30$ eV. However, for the range of 20 eV > T_e > 5 eV the probe and spectroscopic measurements agree remarkably, including the sharp, almost bifurcated reduction of T_e for $<n_e>_{edge}$ below the detachment onset density which is consistent with recent observations in JET L-mode and high-confinement mode (H-mode) plasmas [20], and resembles a similar T_e dependence on $n_{e,sep,LFS\text{-}mp}$ in DIII-D (H-mode) plasmas observed with Divertor Thomson scattering [21].

The saturation of $I_{div,LFS\text{-}plate}$, which is associated with the onset of detachment, coincided with a $<T_e>_{LFS\text{-}div}$ of 2–3 eV (Fig. 2b). The lower bound of $<T_e>_{LFS\text{-}div}$ decreased to 0.5–0.7 eV at the highest $<n_e>_{edge}$ indicating strongly recombining plasmas. (The upper bound of $<T_e>_{LFS\text{-}div}$ is centered at approximately 1.2 eV, which is inherent to the spectroscopic analyses as described in [17]). For $<n_e>_{edge}$ larger than detachment onset density, the spectroscopically inferred n_e across the LFS divertor, $<n_e>_{LFS\text{-}div}$, increased with increasing $<n_e>_{edge}$ up to 6-$8x10^{20}$ m^{-3} and then decreased when $<T_e>_{LFS\text{-}div}$ reached 1 eV, or less, indicating the shift of the high-density region from the strike zone to the LFS divertor X-point (Fig. 2c, also Fig. 4 in [16] and Fig. 4 in [11]). The movement of the high-density region was observed by a radial inward shift across the spectrometer chords, which is interpreted as a poloidal shift from the LFS strike line toward the LFS X-point region, and is consistent with plasma imaging using tangential cameras and Balmer emission line ratios [11,22]. While $<n_e>_{LFS\text{-}div}$ were identical for the pumped and unpumped plasmas at their peak values, $<n_e>_{LFS\text{-}div}$ in the unpumped plasma peaked at 10 % lower $<n_e>_{edge}$ than the pumped plasma. Furthermore, the unpumped plasma exhibited an approximately 20 % lower $<n_e>_{LFS\text{-}div}$ than the pumped plasma in partially detached conditions. This small discrepancy can be explained by a $\lesssim$5 mm radial offset of the strike line at the LFS plate between the two plasmas.

The line-average electron pressures across the LFS divertor, $<p_e>_{LFS\text{-}div}$, derived from $<T_e>_{LFS\text{-}div}$ and $<n_e>_{LFS\text{-}div}$, followed the same trajectory as $<n_e>_{LFS\text{-}div}$ (not shown). Since $<n_e>_{LFS\text{-}div}$ and $<p_e>_{LFS\text{-}div}$ are line-integrated measurements, and $j_{sat,LFS\text{-}plate}$ and $I_{div,LFS\text{-}plate}$ determined at the sheath entrance, it is also conceivable that plasma pressure is lost at the surface at lower $<n_e>_{edge}$ than in the region adjacent to the plate. These observations are independent of the status of the divertor cryogenic pump.

Spectroscopic measurements of the Balmer-α emission across the outer divertor show that the intensities are indistinguishably the same for the pumped and unpumped cases indicating that the D atomic densities at the strike zone, and potentially also in the LFS divertor corner, are the same despite the 5 times higher D_2 pressure in the sub-divertor (not shown). These results suggest that the plasma conditions in the LFS divertor are independent from the sub-divertor molecular pressure, and that pumping raises the fuel throughput only thereby allowing better plasma density control. Since the gas injection rates in unpumped (10^{21} D/s) and pumped (10^{22} D/s) plasmas are factors of 100 and 10 lower than the recycling rates at the divertor plates (10^{23} D/s), respectively, these results reinforce the dominant role of recycling in fueling the core plasma and setting the core plasma density for these plasmas, but likely also for other L-mode and H-mode plasmas.

In many of the discharges the JET machine protection system terminated neutral beam heating prior to the physical density limit. Thus, for both the pumped and unpumped deuterium discharges, the physical density limit could not yet be determined.

4. Detachment onset of the LFS divertor plasma in unpumped D, T and D-T L-mode plasmas

The upstream density ($<n_e>_{edge}$) required to detach the LFS divertor plasma in unpumped D, T and D-T L-mode plasmas was found to be identical for $I_{div,LFS\text{-}plate}$, $<T_e>_{LFS\text{-}div}$ and $<n_e>_{LFS\text{-}div}$ within the uncertainties of the measurement (Fig. 3). Like in pumped and unpumped deuterium discharges, the LFS divertor plasma undergoes a transition from 25 eV to 5 eV over a range of $<n_e>_{edge}$ from $2.0x10^{19}$ m^{-3} to $2.6x10^{19}$ m^{-3}, during which $I_{div,LFS\text{-}plate}$ increased and saturated at $<n_e>_{edge}$ of approximately 2.6 $x10^{19}$ m^{-3} (Fig. 3a), and at which $<T_e>_{,LFS\text{-}div}$ reached 2–3 eV (Fig. 3b).

$n_{e,LFS\text{-}div}$ increased to 6-$7x10^{20}$ m^{-3} for approximately 20 % higher $<n_e>_{edge}$ than the detachment onset density, and decreases for higher $<n_e>_{edge}$ when $<T_e>_{,LFS\text{-}div}$ is 1 eV, or less (Fig. 3c). While $I_{div,LFS\text{-}plate}$ (and $j_{sat,LFS\text{-}plate}$, Fig. 4a) at the detachment onset were identical for the T and D-T plasmas, both parameters were 20 % higher for the D plasma. For $<n_e>_{edge}$ larger than the detachment onset density, the LFS divertor plasma transitions from partial detachment to the density limit over a range of $3x10^{19}$ m^{-3} of $<n_e>_{edge}$. Similar radial shifts of the high-density regions across the spectrometer chords, interpreted as poloidal movement of the high-density region from the LFS strike line to the LFS X-point region, were observed in the D, T and D-T plasmas. Within the uncertainties of how the density limit is established and determined, the limit for the T and D-T plasmas was observed at $<n_e>_{edge} \approx 5.4x10^{19}$ m^{-3}.

Nearly identical plasma conditions were obtained for $<n_e>_{edge}$ at the detachment onset density for $<T_e>_{LFS\text{-}div}$ and $<n_e>_{LFS\text{-}div}$ in D, T and D-T plasmas (Fig. 4b and c), while $j_{sat,LFS\text{-}plate}$ (Fig. 4a) and, consistently, Balmer-α emission across the LFS divertor are 20–30 % higher for D than D-T (Fig. 4b). The fact that the peak $I_{div,LFS\text{-}plate}$ and $j_{sat,LFS\text{-}plate}$ is 10 % higher in the D plasma than in the T and D-T plasmas (Fig. 3a and Fig. 4a, respectively), while $<T_e>_{LFS\text{-}div}$ and $<n_e>_{LFS\text{-}div}$ are nearly identical can be attributed to the fact that $j_{sat,LFS\text{-}plate}$ is local to the target plate, and $<T_e>_{LFS\text{-}div}$ and $<n_e>_{LFS\text{-}div}$ are line-averaged quantities. The root cause for the 20 % difference in the Balmer-α emission is currently unknown, and could be explained by a 10 % lower or higher assumed detachment onset density upstream for the D plasma due to the non-linearity of the divertor plasma on the upstream conditions at the detachment onset. Radial outboard of the separatrix $<T_{e,}>_{LFS\text{-}div}$ was spectroscopically inferred to be 2.2 eV, rising to 3–5 eV poloidally upstream of the strike zone ($R_{LOS,LFS\text{-}plate} < 2.7$ m) and radial outboard of the 2.2 eV region ($R_{LOS,LFS\text{-}plate} > 2.8$ m) (Fig. 4c, see also Fig. 2 in [20]). At the onset of detachment, the spectroscopically inferred $<n_e>_{LFS\text{-}div}$ peaked at the separatrix at a value of $5x10^{20}$ m^{-3} for D, T and D-T (Fig. 4d). In these conditions, the LFS plasmas are observed to be identical for D, T, and D-T.

5. HFS and LFS detachment in H, D, T and D-T pumped and unpumped configurations

Langmuir probe measurements of I_{div} in fuelling ramps from low-recycling conditions to the density limit in pure-protium plasma with the divertor cryogenic pump engaged show the same functional dependence of I_{div} with $<n_e>_{edge}$ as D, T and D-T, including, within 10

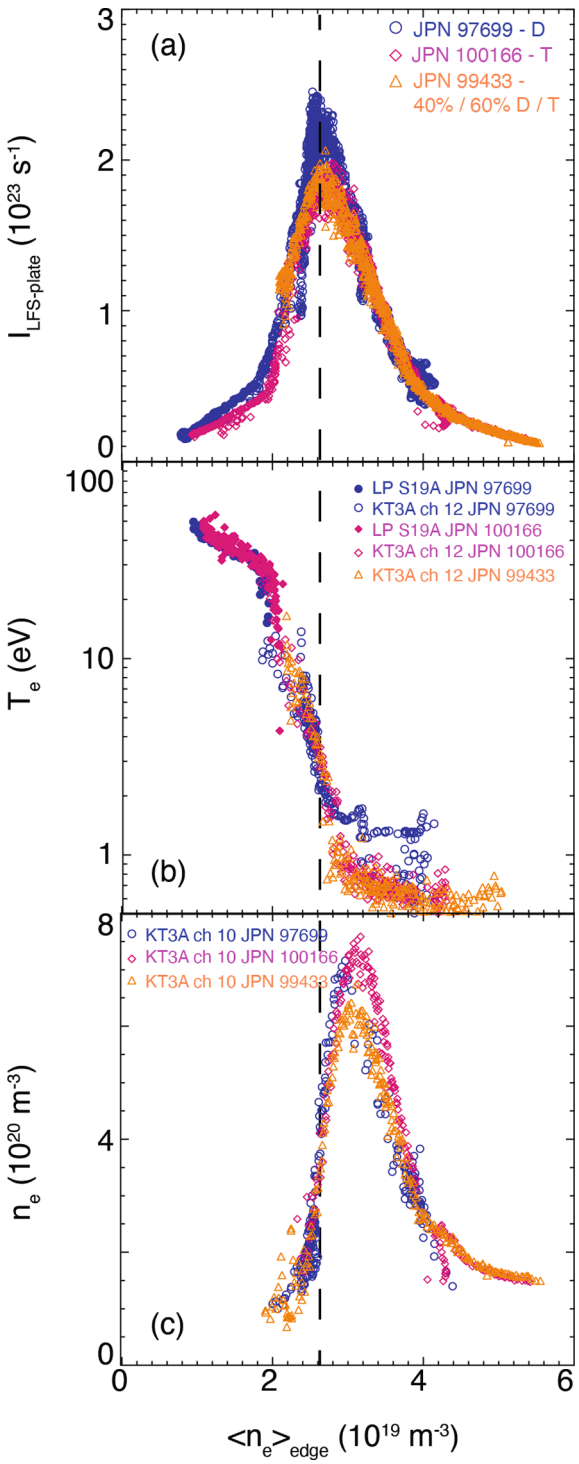

Fig. 3. Total ion current to the LFS target plate (a), electron temperature (b) and electron density (c) as a function of line-averaged density at the outer edge of the core plasma in unpumped plasmas. Deuterium plasmas are shown in blue (JPN 97699), tritium in magenta (JPN 100166) and deuterium–tritium in gold (JPN 99433). T_e (b) was measured with Langmuir probes (circles, probe S19A) and inferred spectroscopically (KT3A, squares, channel 12), while n_e was inferred spectroscopically only (KT3A, squares, channel 10). The black dashed vertical line indicates the assumed detachment onset density based on the saturation of $I_{div,LFS-plate}$. (For interpretation of the references to colour in this figure legend, the reader is referred to the web version of this article.)

%, the same detachment onset density at both the HFS (Fig. 5a) and LFS target plate (Fig. 5b). Fig. 5 combines the pumped and unpumped datasets, highlighting the insensitivity of both $I_{div,HFS-plate}$ and $I_{div,LFS-plate}$ on the status of the divertor cryogenic pump. The observations were made despite cross-field (radial $\mathbf{E} \times B_T$) drifts consistently predict preferentially transport of fuel ions from the LFS to the HFS divertor across the private flux region, and the vertical alignment of the HFS plate versus the horizontal alignment of the LFS plate (e.g., [23]). At the onset of detachment, the j_{sat} profiles for the unpumped D, T and DT plasmas at the HFS and LFS plates were found identical within the uncertainties of the measurements and equilibrium reconstructions (not shown), hence the impact of poloidal cross-field on the HFS and LFS divertor asymmetries is likely more pronounced on T_e and n_e, as observed in other tokamaks (e.g., as directly measured with Divertor Thomson Scattering in DIII-D [24]), and not on j_{sat} and $I_{div,plate}$. Because of sparser dataset of measurements at the HFS target plate and across the HFS divertor leg, and the brevity of this publication, a more detailed comparison of the HFS and LFS divertor plasma conditions is deferred to future publications.

The absolute magnitude of $I_{div,HFS}$ and $I_{div,LFS}$ at the detachment onset density varied approximately by 50 % and 10 %, respectively, without an apparent correlation between the isotope species: the unpumped D case had the highest and the unpumped DT case has the lowest $I_{div,HFS}$. However, for partially detached plasmas at both plates, I_{div} is approximately a factor of 2 higher in H than in D, T and D-T plasmas. The H plasmas have a 20 % higher density limit than the T and D-T plasmas. These observations are consistent with previous measurements in JET-C L-mode [6] and JET-ILW ohmic plasmas in H and D [7]. Given the brevity of the paper, the physics explanations of both findings for these plasmas are outside the scope of this work and deferred to future publications.

6. Summary and discussion

Measurements in JET ITER-like wall, low-confinement mode plasma of high plasma purity and negligible impurity radiation showed that the transition to and density at the onset of detachment in protium, deuterium and tritium plasmas, and deuterium–tritium plasmas of fraction 40 %/60 % are identical within the uncertainties of these measurements. The density limit in protium plasmas was measured to be 20 % higher than in tritium and the deuterium–tritium plasmas. The chosen divertor plasma configuration was a configuration with the LFS strike line connected to the horizontal part of the LFS divertor, which already in JET-C L-mode plasmas [6] and in JET-ILW ohmic plasmas [7] showed little to no dependence (<10 %) on the isotope species. However, in these studies the configuration was chosen for its superior diagnostics coverage. The ion saturation current densities and plate-integrated currents increased and saturated with the same functional dependence on the line-averaged electron density across the LFS edge of the core plasma. These conclusions are independent of the cryogenic pump status, despite a factor of 5 higher sub-divertor pressure of the hydrogenic molecules in unpumped conditions. This result refutes, in part, the hypothesis brought forward in [7] that higher (absolute) sub-divertor pressures as observed in vertical divertor plasma configurations lead to a stronger isotope effect on the detachment onset density. The root cause of these invariances is currently not conclusively identified: previous EDGE2D-EIRENE simulations of H and D ohmic plasmas [7] showed that the pressure differential between the divertor and sub-divertor, and thus the gas flow through the pump duct leads to 40 % higher molecular pressures at the LFS target plate for D versus H (Fig. 6b in Ref. [7]). This result is generally consistent with the lower vacuum conductance for H molecules compared to D molecules in the molecular flow regime valid at sub-divertor pressures of 0.2 Pa. However, the impact of the difference in molecular pressure on the total ion current to the LFS was already shown negligible for ohmic plasmas (Fig. 7a in Ref. [7]). Further studies using both standalone EIRENE to better

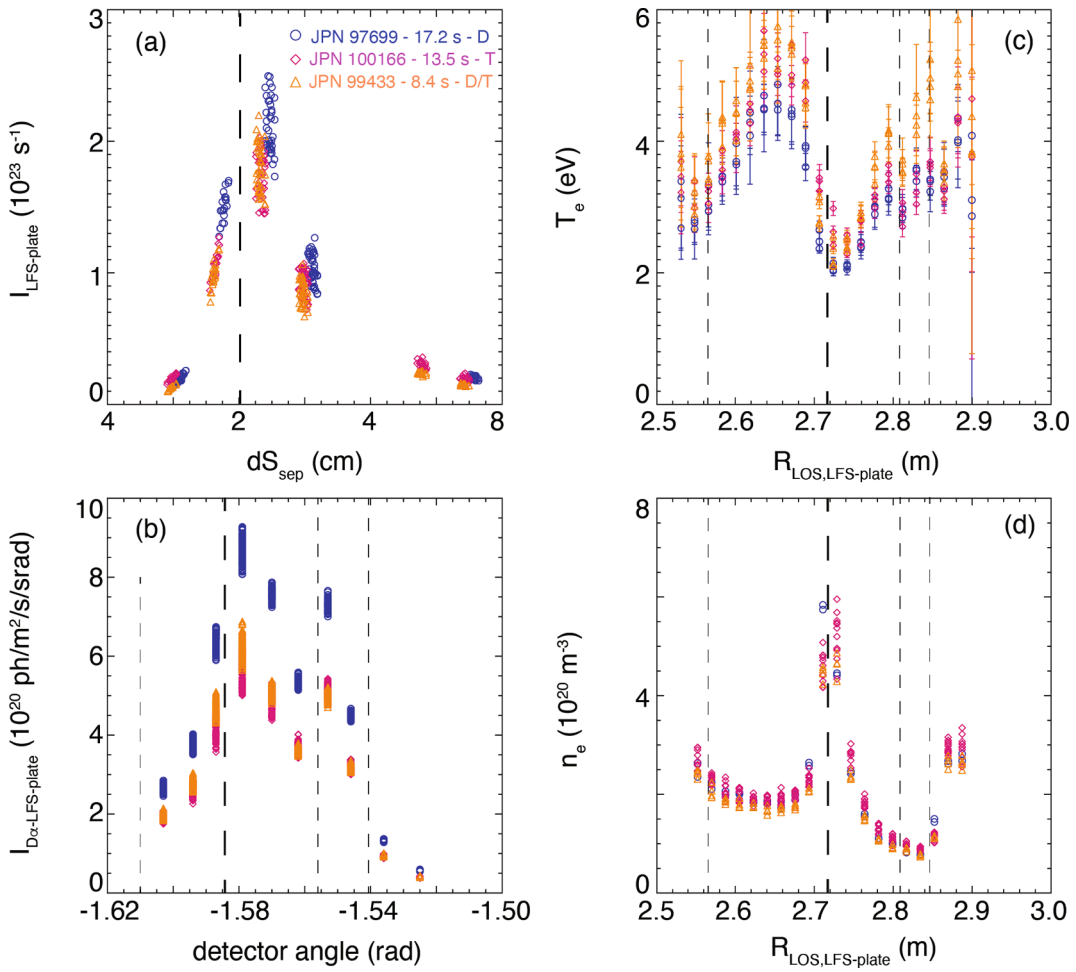

Fig. 4. Radial profiles of the ion saturation current to the LFS plate as a function of distance from the separatrix (a), Balmer-α intensity across the LFS divertor plasma as a function of detector angle (b), and line-averaged $<T_e>_{LFS\text{-}div}$ (c) and $<n_e>_{LFS\text{-}div}$ (d) across the LFS divertor plasmas as a function of radial location of the intersection point of the line-of-sight with the LFS divertor plate at the detachment onset density ($<n_e>_{LFS\text{-}mp} \approx 2.6\text{x}10^{19}$ m^{-3}). Deuterium plasmas are shown in blue (JPN 97699 at 17.2 s), tritium in magenta (JPN 100166 at 13.5 s) and deuterium–tritium in gold (JPN 99433 at 8.4 s). In (b)-(d), the separatrix location is indicated by the thicker dashed black line, while the thinner black dashed lines indicate the radial locations of the innermost and outermost edges of the LFS horizontal plate, and innermost edge of the LFS vertical plate. (For interpretation of the references to colour in this figure legend, the reader is referred to the web version of this article.)

characterize the JET vacuum system and EDGE2D-EIRENE to isolate the physics described in section I are required. Secondly, the studies in both the ohmic and L-mode plasmas rely on the line-averaged density in the edge of the core plasma, $<n_e>_{edge}$, being sufficiently representative for the plasma density, pressure and collisionality at the LFS midplane SOL, including at the separatrix. Despite the high-quality data obtained in these plasmas, the uncertainty in the separatrix location and the general inability to accurately determine the plasma conditions at the separatrix potentially prevent the experimental resolution of the isotope effect on the detachment onset density in these plasmas.

For the subset of the unpumped deuterium, tritium and deuterium–tritium plasmas, the electron temperature spectroscopically inferred across the plasma adjacent to the LFS strike line decreased from 25 eV to 5 eV over a narrow range of increasing core plasma density, and the ion currents saturated when the electron temperature reached 2–3 eV. For core plasma densities higher than the detachment onset density the line-averaged electron density spectroscopically inferred in front of the LFS target increased and then decreased, when the electron temperature reached 1 eV, or less. In this density range, the (spectroscopically inferred) electron pressure followed the trend of the electron density. For currently unknown reasons, but within the uncertainties of the assumed core plasma density, at the onset of detachment the ion saturation current density and the Balmer-α emission are 20–30 % lower for tritium and deuterium–tritium plasmas. The non-linearity of the divertor plasma conditions on the core plasma conditions at the onset of detachment when selecting the time representing the detachment onset in a fuelling ramp is one source of uncertainty that could explain the difference in ion saturation current density and Balmer-α emission without invoking a physics model.

These datasets provide one of the most stringent tests for SOL codes, such as SOLPS-ITER and EDGE2D-EIRENE, not only to elucidate the isotope effect in JET and other tokamaks, but also to validate the plasma and neutral distributions in the divertor SOL, the gas flow through the pump ducts, and the pumping efficiency of the cryogenic pump. As shown in previous publications for deuterium plasmas [7,10,12], both SOLPS-ITER and EDGE2D-EIRENE underpredict the measured electron density at the LFS target plate at the onset of detachment by a factor of 2 to 3 for both H and D plasmas. The resolution of this particular issue precedes the more complete understanding of the isotope effect on the onset of detachment. These studies, however, aid elucidating the impact of the different hydrogenic isotopomers on the onset of detachment, by improving the atomic and molecular input databases to SOLPS-ITER and EDGE2D-EIRENE [5]. These databases currently utilise dissociation, ionisation and recombination rates inferred from hydrogen only, which are scaled by the isotope mass for the main ion–molecule reactions.

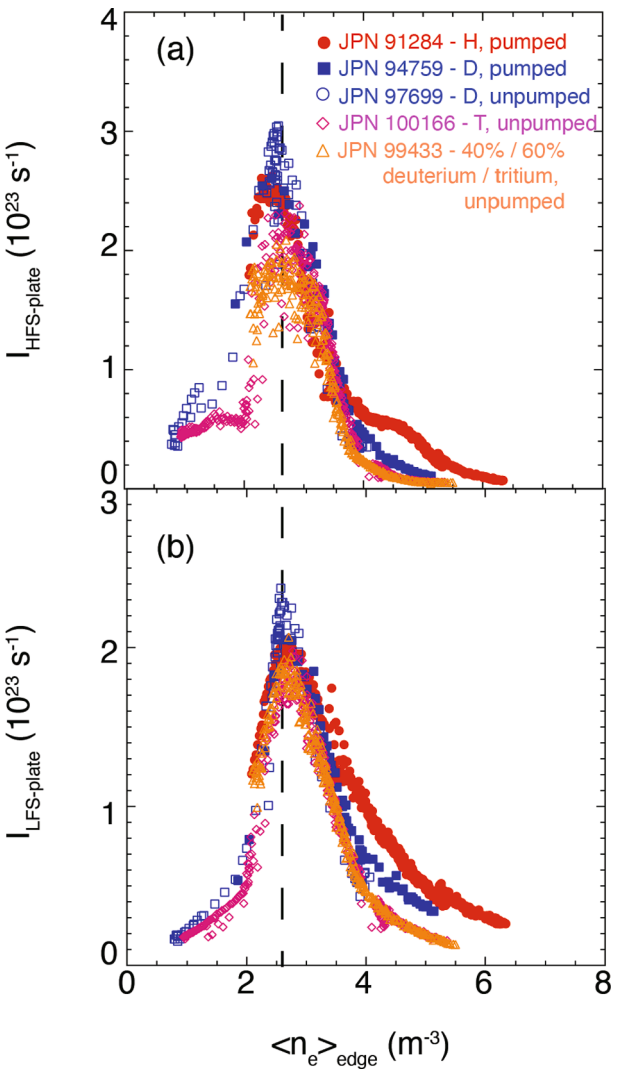

Fig. 5. Total ion current to the HFS (a) and LFS (b) target plate as a function of line-averaged density at the outer edge of the core plasma for hydrogen plasmas (red, JPN 91284), deuterium plasmas (blue, JPNs 94759 and 97699), tritium (magenta, JPN 100166) and deuterium–tritium (gold, JPN 99433). Pumped discharges are indicated by the solid symbols and unpumped discharges by the open symbols. The black dashed vertical line indicates the assumed detachment onset density. (For interpretation of the references to colour in this figure legend, the reader is referred to the web version of this article.)

CRediT authorship contribution statement

M. Groth: Conceptualization, Methodology, Software, Validation, Formal analysis, Investigation, Data curation, Writing – original draft, Writing – review & editing, Visualization, Project administration, Funding acquisition. **V. Solokha:** Methodology, Software, Validation, Formal analysis, Investigation, Data curation, Visualization. **S. Aleiferis:** Methodology, Software, Validation, Formal analysis, Investigation, Data curation, Visualization. **S. Brezinsek:** Conceptualization, Methodology, Software, Validation, Formal analysis, Investigation, Data curation, Writing – review & editing, Visualization, Project administration, Funding acquisition. **M. Brix:** Methodology, Software, Validation, Formal analysis, Investigation, Data curation, Visualization. **I.S. Carvalho:** Methodology, Investigation, Writing – review & editing, Visualization. **P. Carvalho:** Methodology, Software, Validation, Formal analysis, Investigation, Data curation, Visualization. **G. Corrigan:** Methodology, Software, Validation, Investigation, Data curation, Visualization. **D. Harting:** Methodology, Software, Validation, Investigation, Data curation, Visualization. **N. Horsten:** Methodology, Software, Validation, Formal analysis, Investigation, Data curation, Writing – review & editing, Visualization. **I. Jepu:** Methodology, Software, Validation, Formal analysis, Investigation, Data curation, Visualization. **J. Karhunen:** Methodology, Software, Validation, Formal analysis, Investigation, Data curation, Visualization. **K. Kirov:** Methodology, Investigation, Visualization. **B. Lomanowski:** Methodology, Software, Validation, Formal analysis, Investigation, Data curation, Writing – review & editing, Visualization. **K.D. Lawson:** Methodology, Software, Validation, Formal analysis, Investigation, Data curation, Visualization. **C. Lowry:** Methodology, Investigation, Visualization. **A. G. Meigs:** Methodology, Software, Validation, Formal analysis, Investigation, Data curation, Visualization. **S. Menmuir:** Methodology, Software, Validation, Formal analysis, Investigation, Data curation, Visualization. **E. Pawelec:** Methodology, Software, Validation, Formal analysis, Investigation, Data curation, Visualization. **T. Pereira:** Methodology, Software, Validation, Formal analysis, Investigation, Data curation, Visualization. **A. Shaw:** Methodology, Software, Validation, Formal analysis, Investigation, Data curation, Visualization. **S. Silburn:** Methodology, Software, Validation, Formal analysis, Investigation, Data curation, Visualization. **B. Thomas:** Methodology, Software, Validation, Formal analysis, Investigation, Data curation, Visualization. **S. Wiesen:** Methodology, Software, Validation, Formal analysis, Investigation, Data curation, Visualization. **P. Börner:** Methodology, Software, Validation, Formal analysis, Investigation, Data curation, Visualization. **D. Borodin:** Methodology, Software, Validation, Formal analysis, Investigation, Data curation, Visualization. **S. Jachmich:** Methodology, Software, Validation, Formal analysis, Investigation, Data curation, Visualization. **D. Reiter:** Methodology, Software, Validation, Formal analysis, Investigation, Data curation, Visualization. **G. Sergienko:** Methodology, Software, Validation, Formal analysis, Investigation, Data curation, Visualization. **Z. Stancar:** Methodology, Investigation, Visualization. **B. Viola:** Methodology, Software, Validation, Formal analysis, Investigation, Data curation, Visualization. **P. Beaumont:** Methodology, Investigation, Visualization. **J. Bernardo:** Methodology, Investigation, Visualization. **I. Coffey:** Methodology, Software, Validation, Formal analysis, Investigation, Data curation, Visualization. **N.J. Conway:** Methodology, Investigation, Visualization. **E. de la Luna:** Methodology, Software, Investigation, Data curation, Visualization, Supervision, Project administration. **D. Douai:** Methodology, Investigation, Data curation, Supervision, Project administration. **C. Giroud:** Methodology, Software, Validation, Formal analysis, Investigation, Data curation, Visualization. **J. Hillesheim:** Methodology, Investigation, Data curation, Supervision, Project administration. **L. Horvath:** Methodology, Investigation, Visualization. **A. Huber:** Methodology, Software, Investigation, Data curation, Visualization, Supervision, Project administration. **P. Lomas:** Methodology, Investigation, Visualization. **C.F. Maggi:** Methodology, Software, Investigation, Data curation, Visualization, Supervision, Project administration. **M. Maslov:** Methodology, Investigation, Visualization. **C. Perez von Thun:** Methodology, Investigation, Visualization. **S. Scully:** Methodology, Software, Validation, Formal analysis, Investigation, Data curation, Visualization. **N. Vianello:** Methodology, Investigation, Data curation, Supervision, Project administration. **M. Wischmeier:** Methodology, Investigation, Data curation, Supervision, Project administration.

Declaration of Competing Interest

The authors declare the following financial interests/personal relationships which may be considered as potential competing interests: [Mathias Groth reports financial support was provided by European Consortium for the Development of Fusion Energy.].

Data availability

Data will be made available on request.

Acknowledgements

This work has been carried out within the framework of the EUROfusion Consortium, funded by the European Union via the Euratom Research and Training Programme (Grant Agreement No 101052200 — EUROfusion). Views and opinions expressed are however those of the author(s) only and do not necessarily reflect those of the European Union or the European Commission. Neither the European Union nor the European Commission can be held responsible for them.

This scientific paper has been published as part of the international project co-financed by the Polish Ministry of Science and Higher Education within the programme called 'PMW' for 2020-22.

References

[1] ITER Physics Expert Group on Divertor et al., Chapter 4: Power and particle control, Nucl. Fus. **39** (1999) 2391.
[2] A. Loarte, B. Lipschultz, A.S. Kukushkin, G.F. Matthews, P.C. Stangeby, N. Asakura, G.F. Counsell, G. Federici, A. Kallenbach, K. Krieger, A. Mahdavi, V. Philipps, D. Reiter, J. Roth, J. Strachan, D. Whyte, R. Doerner, T. Eich, W. Fundamenski, A. Herrmann, M. Fenstermacher, P. Ghendrih, M. Groth, A. Kirschner, S. Konoshima, B. LaBombard, P. Lang, A.W. Leonard, P. Monier-Garbet, R. Neu, H. Pacher, B. Pegourie, R.A. Pitts, S. Takamura, J. Terry, E. Tsitrone, T.-O. Group, Chapter 4: Power and particle control, Nucl. Fusion 47 (6) (2007) S203–S263.
[3] R.A. Pitts, et al., Nucl. Mater. Energy 20 (2019), 100969.
[4] Chr. Day et al., Fus. Eng. Des. **69** (2003) 97.
[5] R.K. Janev, D. Reiter, Berichte des Forschungszentrums Jülich, Jül-4411, ISSN 0944-2952 (2018).
[6] C.F. Maggi, et al., Nucl. Fusion 39 (1999) 979.
[7] V. Solokha, et al., Nucl. Mater. Energy 25 (2020), 100836.
[8] J. Mailloux, et al., Nucl. Fusion 62 (2022), 042026.
[9] W. Obert et al., Fusion Technology 1991, Proc. 16th Symposium on Fusion Technology, London, U.K., 3–7 September 1990 (1991) 488-492.
[10] M. Groth, et al., Nucl. Fusion 53 (2013), 093016.
[11] J. Karhunen, et al., Plasma Phys. Controlled Fusion 63 (2021), 085018.
[12] N. Horsten, et al., Nucl. Mater. Energy 33 (2022), 101247.
[13] V.S. Neverov, et al., Nucl. Fusion 59 (2019), 046011.
[14] C.C. Klepper, et al., Nucl. Fusion 60 (2020), 016021.
[15] G.J. van Rooij, et al., J. Nucl. Mater. 438 (2013) S42.
[16] A.G. Meigs, et al., J. Nucl. Mater. 438 (2013) S607.
[17] B. Lomanowski, et al., Nucl. Fusion 55 (2015), 123028.
[18] K.D. Lawson, et al., Nucl. Mater. Energy 12 (2017) 924.
[19] M. Groth, et al., J. Nucl. Mater. 438 (2013) S175.
[20] B. Lomanowski, et al., Nucl. Fusion 62 (2022), 066030.
[21] A.G. McLean, et al., J. Nucl. Mater. 463 (2015) 533.
[22] J. Karhunen et al., this conference.
[23] A.V. Chankin, et al., Plasma Phys. Controlled Fus. 36 (1994) 1853.
[24] T.D. Rognlien, et al., Nucl. Mater. Energy 12 (2017) 44.